Noise-induced synchronization of spin-torque oscillators

Yusuke Imai,[1,*] Sumito Tsunegi,[1,2] Kohei Nakajima,[3] and Tomohiro Taniguchi[1,†]

[1]*National Institute of Advanced Industrial Science and Technology (AIST), Research Center for Emerging Computing Technologies, Tsukuba, Ibaraki 305-8568, Japan*

[2]*PRESTO, Japan Science and Technology Agency (JST), Saitama 332-0012, Japan*

[3]*Graduate School of Information Science and Technology, The University of Tokyo, Bunkyo-ku 113-8656, Tokyo, Japan*

(Received 13 March 2022; revised 6 June 2022; accepted 6 June 2022; published 15 June 2022)

Noise-induced synchronization is a phenomenon where several oscillators with different initial conditions show synchronized motion, even in the absence of a coupling between them, when common stochastic input signals are injected. The phenomenon has attracted attention from nonlinear science, as well as applied physics, because it enables environmental noise to be used to synchronize many oscillators and is a necessary condition for brain-inspired computing. Here we develop a theoretical analysis of noise-induced synchronization in spin-torque oscillators (STOs). The analytical form for the Lyapunov exponent for the present model we derive indicates that there are two contributions from input signal to noise-induced synchronization in STOs. The first is that the input signal directly aligns the phases of the magnetizations, and the second is that the input signal changes the oscillating amplitude, and the amplitude-phase coupling results in synchronization. The validity of the analytical results was qualitatively confirmed by numerical simulation. We also show the existence of on-off intermittency at finite temperature, whose statistical properties are similar to those of other oscillator systems.

DOI: 10.1103/PhysRevB.105.224407

I. INTRODUCTION

A spin-torque oscillator (STO) is a nonlinear oscillator on the nanoscale in which spin-transfer torque [1–3] excited in a ferromagnetic/nonmagnetic multilayer drives oscillation of the magnetization at a frequency in the range of 100 MHz–10 GHz [4–33]. It is of both fundamental and practical interest because it is an example of a limit-cycle oscillator [34–36] and potentially has device applications such as in the recording heads of high-density hard-disk drives [37] and physical reservoir computing [38]. A fascinating phenomenon of nonlinear oscillators is synchronization, where several oscillators show frequency and/or phase synchronization. Two mechanisms for this synchronization have mainly been investigated. The first is mutual synchronization, where STOs are synchronized through several coupling mechanisms such as dipole interaction and spin-wave propagation [8,9,28,31,32]. The other mechanism is forced synchronization, where the frequency and phase of the STOs are locked by an external or self-feedback signal [7,21,30].

In the field of nonlinear science, another mechanism of synchronization, namely, noise-induced synchronization, has been investigated in various oscillator systems [35,39–43]. Noise-induced synchronization is a phenomenon in which several oscillators with different initial conditions show synchronized motion when common stochastic signals are injected. Here, noise and stochastic signal mean (pseudo) random input in the form of, for example, electric voltage, which can be applied to several oscillators simultaneously and/or be reproducibly applied to an oscillator. Therefore, noise and stochastic input signal here are different from, for example, thermal fluctuation in ferromagnets [44]: thermal noise originates from the internal nature of each oscillator, and thus its value is independent among the oscillators and cannot be reproduced. Noise-induced synchronization is classified as generalized synchronization, where the state of oscillators is determined by the state of the driving system [35]. The phenomenon is different from mutual synchronization because interactions among the oscillators are unnecessary for it to occur. It also differs from forced synchronization because the input signal does not have periodicity. Noise-induced synchronization is not only of fundamental interest but also of practical interest because it enables many oscillators to be synchronized by, for example, environmental noise without power injection. Recently, noise-induced synchronization has attracted attention in the field of brain-inspired computing because it guarantees the computational reproducibility, called the echo-state property, of physical reservoir computing [45–47]. However, only a few studies on noise-induced synchronization in STOs have been reported [47–49]. In addition, the previous work performed numerical simulations at zero temperature only, and the physical mechanism causing the synchronization and the role of temperature have not been revealed.

In this work we develop a theoretical analysis of noise-induced synchronization in STOs. We focus on a magnetic-vortex-type STO that has been used in recent experiments [38,50,51] and use a stochastic magnetic field as input signal. First we perform a numerical simulation of the magnetization dynamics at zero temperature and find that synchronization

*imai-yusuke@aist.go.jp
†tomohiro-taniguchi@aist.go.jp

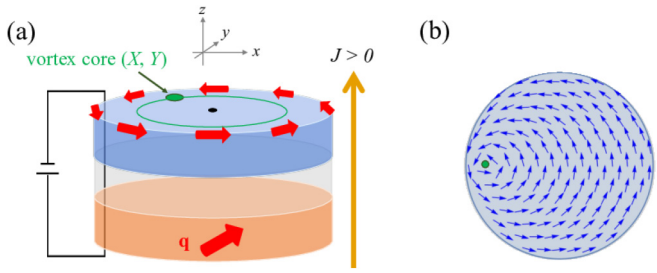

FIG. 1. (a) Schematic illustration of a magnetic-vortex STO. The top (blue) ferromagnetic layer corresponds to the free layer, while the bottom (orange) ferromagnetic layer corresponds to the reference layer. The position of the vortex core in the free layer is $\mathbf{X} = (X, Y, 0)$, while the unit vector pointing in the direction of magnetization in the reference layer is $\mathbf{q}$. (b) Example of the magnetic profile in the free layer, where the direction of the magnetic moment is evaluated from the profile in Ref. [22].

occurs efficiently when the oscillation amplitude is small or the coupling between the amplitude and phase is large. Second, we derive an analytical form for the Lyapunov exponent for the present model and find that the results of the numerical simulation are well explained by it. The analytical form for the Lyapunov exponent implies that there are two ways to realize the synchronization. The first one is that the input signal of the magnetic field directly aligns the phases of the STOs. The second is that the input signal changes the oscillating amplitude, which leads to phase alignment through the amplitude-phase coupling. Third, we perform a numerical simulation at finite temperature. While synchronization occurs even in the presence of thermal fluctuation, on-off intermittency is also observed. A statistical analysis clarifies that on-off intermittency in the STOs plays a similar role to those found in other oscillator systems.

The paper is organized as follows. In Sec. II we provide a system description and show the oscillatory behavior of the vortex core in the absence of a stochastic input signal. In Sec. III we describe a numerical simulation of noise-induced synchronization at zero temperature. An analytical theory of the synchronization is also developed. In Sec. IV we show the results of a numerical simulation at finite temperature and study the desynchronized behavior statistically. Our conclusions are summarized in Sec. V.

II. SYSTEM DESCRIPTION

Let us describe the STO under investigation.

A. Thiele equation

We will focus on a magnetic-vortex STO consisting of a ferromagnetic/nonmagnetic/ferromagnetic trilayer as schematically shown in Fig. 1(a). The free layer includes a magnetic vortex [Fig. 1(b)], while the reference layer is uniformly magnetized. The z axis is perpendicular to the film plane, while the magnetization in the reference layer is in the xz plane. It has been confirmed [16,22,26,33] that the experimental and numerical results are well described by the Thiele equation [16,52–56]:

$$-G\mathbf{e}_z \times \dot{\mathbf{X}} - |D|(1+\xi s^2)\dot{\mathbf{X}} - \kappa(1+\zeta s^2)\mathbf{X} + a_J J q_z \mathbf{e}_z \times \mathbf{X} + c a_J J R_0 q_x \mathbf{e}_x - c b_J J R q_x \mathbf{e}_y + c\mu^* \mathbf{e}_z \times \mathbf{H} - \eta_x \mathbf{e}_x - \eta_y \mathbf{e}_y = \mathbf{0}, \quad (1)$$

where $\mathbf{e}_i$ is the unit vector representing the i direction, $\mathbf{X} = (X, Y, 0)$ is the position vector of the vortex core, while $G = 2\pi pML/\gamma$ and $D = -(2\pi\alpha ML/\gamma)[1 - (1/2)\ln(R_0/R)]$ consist of the saturation magnetization M, the gyromagnetic ratio γ, the Gilbert damping constant α, the thickness L, the disk radius R, and the core radius R_0. The polarity p and chirality c are each assumed to be $+1$ for convenience. The normalized distance of the vortex-core position from the disk center is $s = |\mathbf{X}|/R = \sqrt{(X/R)^2 + (Y/R)^2}$. The dimensionless parameter ξ was introduced to describe the nonlinear damping in a highly excited state [22], where the strength of the damping torque increases nonlinearly with increasing s. The magnetic potential energy W is characterized by κ and ζ via

$$W = \frac{\kappa}{2}\left(1 + \frac{\zeta}{2}s^2\right)|\mathbf{X}|^2, \quad (2)$$

and $\kappa = (10/9)4\pi M^2 L^2/R$ [22]. The dimensionless parameter ζ was introduced to explain the linear dependence of the oscillation frequency on the current [22]. The spin-transfer torque strength with spin polarization P is $a_J = \pi\hbar P/(2e)$ [16,56], while the fieldlike torque strength is given by b_J. The electric current density is denoted by J, where positive current corresponds to that flowing from the reference to the free layer, as shown in Fig. 1(a). The unit vector pointing in the magnetization direction in the reference layer is $\mathbf{q} = (q_x, 0, q_z)$. The external magnetic field is denoted as $\mathbf{H}$, while $\mu^* = \pi MLR$. The thermal fluctuation provides a random torque, whose components obey the fluctuation-dissipation theorem,

$$\langle \eta_k(t)\eta_\ell(t')\rangle = 2k_B T|D|\delta_{k\ell}\delta(t-t'), \quad (3)$$

where T is temperature. In the following we will use the following values of the parameters found in typical experiments and simulations [22,26,33]: $M = 1300$ emu/c.c., $\gamma = 1.764 \times 10^7$ rad/(Oe s), $\alpha = 0.01$, $L = 5$ nm, $R = 187.5$ nm, $R_0 = 10$ nm, $P = 0.7$, $b_J = 0$, $\xi = 2$, and $\mathbf{q} = (\sin 60^\circ, 0, \cos 60^\circ)$. The values of J and ζ are varied, as mentioned below, because they relate to the ways to realize noise-induced synchronization. A current $I = \pi R^2 J$ of 1 mA corresponds to a current density J of 0.9 MA/cm^2. It was reported that ζ relates to the material and is on the order of 0.1–1.0 [26]. As explained below, the stochastic input signal for the synchronization is injected through the magnetic field, $\mathbf{H}$.

B. Oscillating behavior in the absence of stochastic input signal

Before investigating the synchronization phenomena, let us show the oscillatory behavior in the absence of stochastic input signal through $\mathbf{H}$. The results shown here will be used to develop an analytical theory of synchronization later.

Figure 2(a) shows an example of the time evolution of $s = |\mathbf{X}|/R$ at zero temperature, where the current $I = \pi R^2 J$

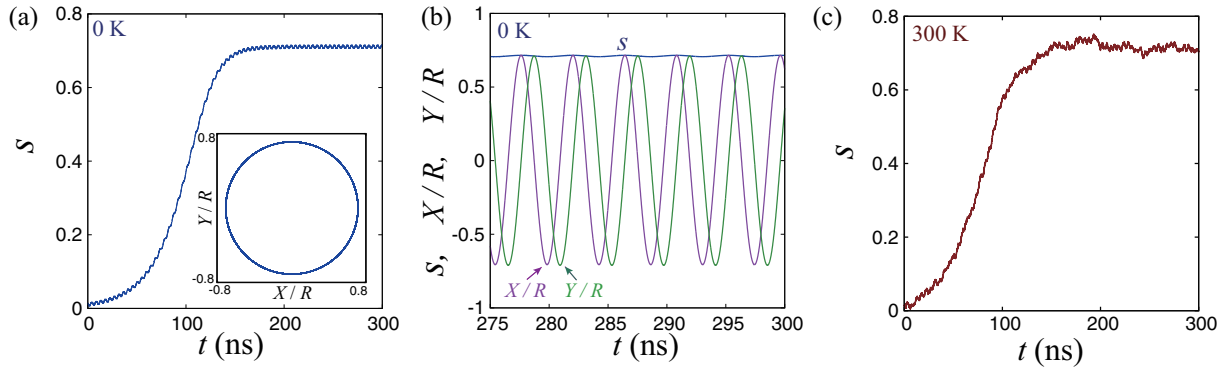

FIG. 2. (a) Time evolution of the normalized distance s from the disk center at zero temperature. The inset shows the dynamical trajectory in the steady state. (b) Oscillating behavior of X and Y at zero temperature. The oscillation frequency is about 226 MHz. (c) Time evolution of the normalized distance at $T = 300\,\mathrm{K}$.

is 5 mA and $\zeta = 0.1$. Starting near the disk center, the vortex core moves to an oscillating state. The normalized distance s of the vortex core approximately saturates to a certain value, which can be confirmed from the inset of Fig. 2(a) showing the dynamical orbit of the vortex core in the steady state. In this sense, s can be regarded as an oscillation amplitude of the vortex core. The small-amplitude oscillation of s originates from the spin-transfer torque due to the in-plane component q_x of $\mathbf{q}$ appearing as the fifth term of Eq. (1), which breaks the axial symmetry of the Thiele equation around the z axis. Figure 2(b) shows the oscillating behavior of X and Y. The frequency is about 226 MHz, which is a typical value for vortex STOs [22,26,33]. Note that the analytical form explaining these dynamical behaviors can be derived from Eq. (1). Neglecting terms related to the small parameters, such as α and R_0/R, the Thiele equation in terms of s and the phase $\psi = \tan^{-1}(Y/X)$ becomes (see also Appendix A)

$$\dot{s} = as - bs^3, \tag{4}$$

$$\dot{\psi} = \frac{\kappa}{G}(1 + \zeta s^2), \tag{5}$$

where a and b are defined as

$$a = \frac{|D|\kappa}{G^2}\left(\frac{J}{J_c} - 1\right), \tag{6}$$

$$b = \frac{|D|\kappa}{G^2}(\xi + \zeta). \tag{7}$$

The critical current density inducing the oscillation is $J_c = |D|\kappa/(Ga_J q_z)$. Note that Eqs. (4) and (5) are the same as the equation of motion of a Stuart-Landau oscillator [36]. The Stuart-Landau equation was derived by Landau to describe the evolution of turbulence phenomenologically, and its derivation from hydrodynamics was developed by Stuart. It provides a simple example of nonlinear dynamical systems having Hopf bifurcation. The solution of s in a steady state is $s_0 = \sqrt{a/b}$, whose value is 0.73 for the present parameter and is close to the value in Fig. 2(a). The oscillation frequency estimated from Eq. (5), $(\kappa/G)(1 + \zeta s_0^2)/(2\pi)$, is also consistent with the numerical simulation in Fig. 2(b). Note as well that the nonlinear parameter ζ of the magnetic potential can be regarded as a coupling between the amplitude and the frequency (phase).

At finite temperature, the thermal fluctuation provides a randomness to $\mathbf{X}$, as can be confirmed from Fig. 2(c) showing the time evolution of s at $T = 300\,\mathrm{K}$. However, the average value of s and the oscillation frequency are approximately the same as their values at zero temperature.

Here we should note that the phase $\psi(t)$ of the vortex-core position, $\mathbf{X}$, in the xy plane at a time t depends on the initial condition. Let us imagine two vortex STOs where the vortex cores, $\mathbf{X}_1$ and $\mathbf{X}_2$, have different phases at a certain time t_0. In this case the phase difference between the two vortex cores does not become smaller because they oscillate with the same frequency. The noise-induced synchronization is a phenomenon in which these vortex-core positions overlap, even if the initial states are different, when a stochastic signal is injected. In the next section we will investigate the phenomenon at zero temperature through a numerical simulation and analytical treatment.

III. SYNCHRONIZATION AT ZERO TEMPERATURE

Here we describe a result of numerical calculation of Eq. (1) that shows the synchronized behavior of the magnetic-vortex cores by injecting a stochastic magnetic field and derive analytical form for the Lyapunov exponent for the present model. The fourth-order Runge-Kutta method is applied to solve Eq. (1) numerically. The temperature is assumed to be zero.

Before showing the results, let us briefly emphasize the concept of noise-induced synchronization again. Synchronization studied previously is mutual or forced synchronization. In mutual synchronization, two (or more) oscillators having identical or close parameters oscillate with the same frequency and fixed phase difference through interactions. In forced synchronization, the oscillation frequency of an oscillator is forcibly changed to that of an external signal. On the other hand, noise-induced synchronization belongs to generalized synchronization. The generalized synchronization was proposed in the middle of the 1990s. For example, Ref. [57] found that dynamical variables of two chaotic systems with a unidirectional interaction have some relation, even though the equations of motions, as well as typical timescales, of the two systems are different and hence the time evolutions

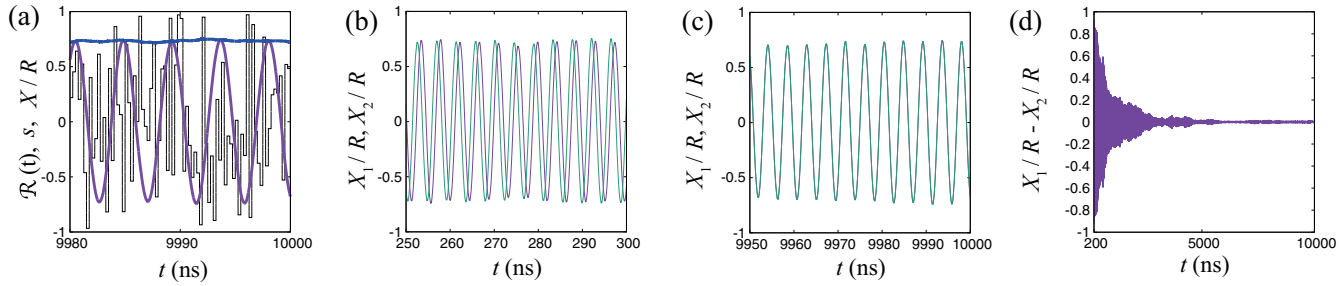

FIG. 3. (a) Examples of X/R, s, and $\mathcal{R}$, where $I = 5.0$ mA, $\zeta = 0.1$, $t_p = 0.25$ ns, and $h_x = 5.0$ Oe. (b), (c) Examples of oscillating behaviors of X/R in two trials (b) immediately after starting the injection of the stochastic signal from $t = 200$ ns and (c) a long time after injection. The time evolution of their difference, $(X_1/R) - (X_2/R)$, is shown in (d). The temperature is zero.

of the dynamical variables of the two systems look different. Even if the dimensions of two systems are different, similar phenomena can be observed. These observations were different from the conventional synchronization, where the dynamical variables of two systems change identically except for the phase difference. Therefore the concept of generalized synchronization was introduced. As will be explained in the following, in the noise-induced synchronization, the frequency of STO does not become identical to that of the input signal: nevertheless, the phases of different oscillators align. In this sense, noise-induced synchronization is classified as generalized synchronization.

A. Numerical simulation

The simulation of Eq. (1) involved solving Eq. (1) for 1000 different initial conditions of the vortex core; see also Appendix B. Note that the STO includes a single vortex, and the equation of motion is solved for the 1000 different initial conditions; i.e., we do not assume 1000 vortex cores in a single STO. In the following we add a suffix $i = 1, 2, \ldots, N$ ($N = 1000$) distinguishing the trials of X and Y as X_i and Y_i when necessary.

We solve Eq. (1) without a magnetic field from $t = 0$ to $t = 200$ ns to move the vortex core to the steady oscillating state. Then we inject a stochastic magnetic field. Note that the stochastic signal is common to the 1000 trials. Note as well that the previous models of noise-induced synchronization have used various stochastic signals, such as Gaussian noise or impulse noise [35,39–43]. Here we assume a pulse signal, which has been used in recent experiments [50,51], in the form of a magnetic field given by

$$\mathbf{H}(t) = h_x \mathcal{R}(t) \mathbf{e}_x, \tag{8}$$

where $\mathcal{R}(t)$ is a uniform random number in the range $[-1, 1]$ and is constant during the pulse width t_p, while h_x determines the maximum value of the input signal. We again emphasize that the stochastic input signal given by Eq. (8) can be simultaneously applied to several oscillators and/or reproducibly applied to an oscillator. In this sense, stochastic input signal here is different from thermal fluctuation in ferromagnet, whose role will be studied in Sec. IV. In addition to noise-induced synchronization, Ref. [47] finds stochastic current-input-driven chaos in a macrospin STO. The phenomenon is beyond the scope of the present work, and we keep it as a future work.

Figure 3(a) shows examples of X/R, s, and $\mathcal{R}$. Comparing s with what is shown in Fig. 2(a), we can see that there is small-amplitude random motion due to the stochastic input signal. We should emphasize here that the vortex core does not synchronize to the input signal, i.e., the oscillation frequency of X/R is different from the timescale of the input signal, such as $1/t_p$. Thus this phenomenon is different from forced synchronization. Figure 3(b) shows the oscillations of two X/R immediately after injecting the stochastic input signal. Since the two trials have different initial conditions, their phases are different. However, after a long time passes, their phases become identical, as can be seen in Fig. 3(c). Figure 3(d) shows the time evolution of the difference in X/R between two trials; the difference rapidly, and approximately monotonically, becomes small. These results indicate that noise-induced synchronization is achieved by injecting a stochastic magnetic field.

To clarify the ways to realize the synchronization, let us investigate the dependence of the synchronized behavior on the parameters. Figure 4 shows the distributions of the vortex-core positions at $t = 10$ μs for 1000 trials. In Fig. 4(a), the current I and the amplitude-phase coupling parameter ζ are identical to those in Fig. 3(a), i.e., $I = 5$ mA and $\zeta = 0.1$. As in the case shown in Fig. 3 for two trials, many of the vortex-core positions overlap, indicating that noise-induced synchronization occurs. Simultaneously, however, there are some trials which are not synchronized even after a long time passes. We note that it does not mean the absence of synchronization; rather, it implies that a time necessary to achieve synchronization is sufficiently long. Notice that synchronization is efficiently achieved in all trials when the current magnitude is reduced, as shown in Fig. 4(b), where $I = 2.5$ mA and $\zeta = 0.1$. Recall that the value of s in a steady state, as estimated from the analytical theory in Sec. II, $s_0 = \sqrt{a/b}$, decreases with decreasing current magnitude through $a \propto J$. Therefore the result shown in Fig. 4(b) indicates that noise-induced synchronization is rapidly achieved when the oscillation amplitude is small. In addition, synchronization is efficiently achieved when the coupling between the amplitude and phase is large. Figure 4(c) shows the distribution of vortex-core positions when ζ is 0.4. Here the increase in ζ makes the oscillation amplitude s small, as implied by the analytical result, $s_0 = \sqrt{a/b} \propto \sqrt{1/(\xi + \zeta)}$. To separate the ways to realize the synchronization from the one shown in Fig. 4(b), we increase the current to $I = 7.5$ mA and simultaneously keep the oscillation amplitude comparable to that in Fig. 4(a). Again, the vortex

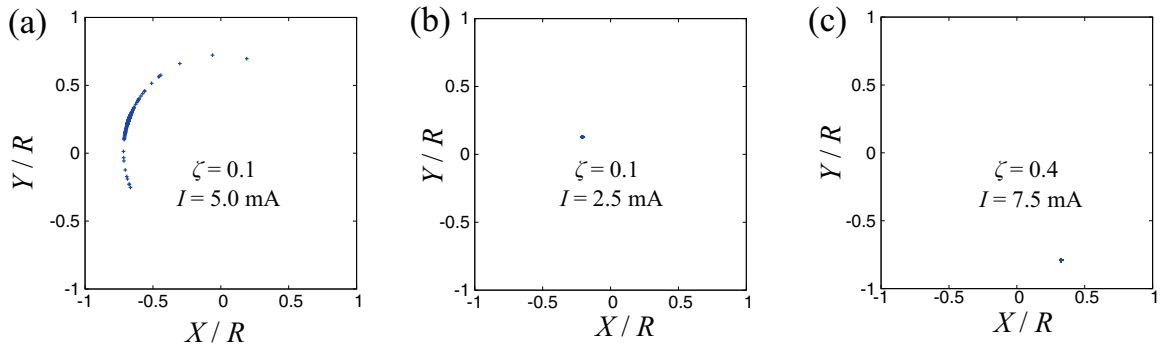

FIG. 4. Distribution of vortex-core positions at $t = 10$ μs, where the values of I and ζ are (a) 5.0 mA and 0.1, (b) 2.5 mA and 0.1, and (c) 7.5 mA and 0.4. The maximum value of the input signal of the magnetic field is $h_x = 5.0$ Oe. The temperature is zero. In (b) and (c), all points are mostly overlapped.

cores of all trials almost completely overlap, indicating the appearance of noise-induced synchronization.

One might be interested in the temporal evolution into the synchronized state. Figure 5 compares the time evolutions of the oscillation amplitude s of a single trial and its average. The average is defined as

$$\bar{s} = \sqrt{\left(\frac{1}{N}\sum_{i=1}^{N}\frac{X_i}{R}\right)^2 + \left(\frac{1}{N}\sum_{i=1}^{N}\frac{Y_i}{R}\right)^2}. \tag{9}$$

According to the definition, $\bar{s}$ becomes small when the vortex cores have different phases and thus $\sum_{i=1}^{N} X_i$ and $\sum_{i=1}^{N} Y_i$ become zero. On the other hand, when synchronization is achieved, $\bar{s}$ becomes identical to the oscillation amplitude of a single trial. The values of I and ζ in Fig. 5 are (a) 5.0 mA and 0.1, (b) 2.5 mA and 0.1, and (c) 7.5 mA and 0.4, as in the case of Fig. 4. Comparing Figs. 5(a) and 5(b), we find that fast synchronization is achieved when the oscillation amplitude is small, where the amplitude of a single trial is almost overlapped by the averaged amplitude in Fig. 5(b). This is because the differences among the vortex-core positions are also small. On the other hand, the times required for $\bar{s}$ to reach a single-trial value of s are nearly the same for the cases shown in Figs. 5(a) and 5(c), although the number of the synchronized vortex cores is different [Figs. 4(a) and 4(c)]. This is because differences among the vortex-core positions can be large when the oscillation amplitude is large; therefore a relatively long time is necessary to achieve synchronization. Note that the strength of the input signal h_x is the same for every plot in Fig. 5, and the dependence of the time for synchronization on the strength of input signal is shown in Appendix C.

B. Analytical theory

The results of the numerical simulation indicate that there are two ways of realizing noise-induced synchronization efficiently. The first one is to reduce the oscillation amplitude s. The second one is to use materials with a large amplitude-phase coupling ζ. Here we develop an analytical theory of the synchronization and reveal the physics behind it.

First, we should note that synchronization among the vortex cores occurs when the torque due to the stochastic input signal depends on the core position; if the torque due to the input signal is independent of the core position, all cores are moved uniformly by the torque, and the distance between them does not decrease. Note that the Thiele equation for s and ψ in the presence of a stochastic input signal, with leading-order terms only, becomes

$$\dot{s} = as - bs^3 + \frac{c\mu^*}{GR} h_x \mathcal{R}(t)\cos\psi, \tag{10}$$

$$\dot{\psi} = \frac{\kappa}{G}(1 + \zeta s^2) - \frac{c\mu^*}{GRs} h_x \mathcal{R}(t)\sin\psi, \tag{11}$$

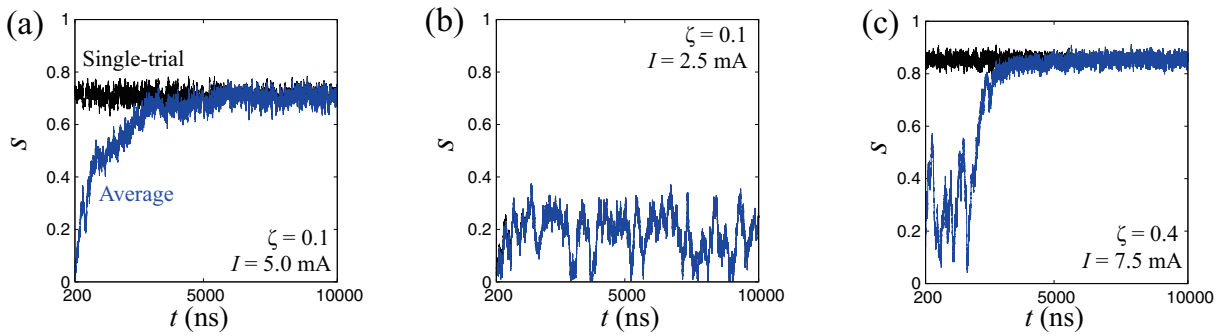

FIG. 5. Time evolutions of the oscillation amplitude s_0 of a single trial (black) and its average (blue), where the values of I and ζ are (a) 5.0 mA and 0.1, (b) 2.5 mA and 0.1, and (c) 7.5 mA and 0.4. The maximum value of the input signal of the magnetic field is $h_x = 5.0$ Oe. The temperature is zero. In (b) the amplitude of a single trial is almost overlapped by the averaged amplitude.

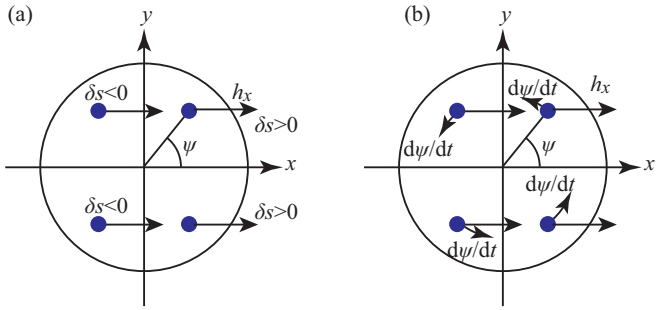

FIG. 6. (a) The arrows indicate the direction of torque due to the magnetic field ($h_x > 0$), while the dots indicate the positions of the vortex core. When the vortex core is in the region of $X > 0$ ($X < 0$), the oscillation amplitude increases (decreases) due to the torque, i.e., the change δs in s from s_0 is positive (negative). (b) Relation between the oscillation and torque directions. When the vortex core is in the region of $Y > 0$ ($Y < 0$), the torque due to the magnetic field has a component antiparallel (parallel) to the rotating direction of the core, which decreases (increases) the instantaneous frequency ($\propto d\psi/dt$).

where we can confirm that the torques acting on s and ψ depend on the core position (phase) through the terms proportional to $h_x\mathcal{R}(t)\cos\psi$ and $h_x\mathcal{R}(t)\sin\psi$. The dependences of these torques on the phase ψ can be explained as follows. According to Eq. (1), the main contribution of the magnetic field is to move the vortex core in the direction of the field, i.e., $\dot{\mathbf{X}} \propto \mathbf{H}$. Let us imagine that the vortex core rotates around the disk center in a counterclockwise direction, as is schematically shown in Fig. 6, where we have assumed that $\mathcal{R} > 0$. In this case the torque due to the magnetic field moves the vortex core in the positive x direction. When the vortex core is located in the region of $X > 0$ ($X < 0$), the torque due to the magnetic field tends to increase (decrease) the oscillation amplitude; see Fig. 6(a), where δs is the change in the oscillation amplitude from s_0. Thus the dependence of the torque acting on s on the phase can be described by a function of $\cos\psi$. Similarly, when the vortex core is in the region of $Y > 0$ ($Y < 0$), the direction of the torque due to the magnetic field has an antiparallel (parallel) component to the oscillating direction, which decreases (increases) the instantaneous frequency of the vortex core; see Fig. 6(b), where the arrows with $d\psi/dt$ indicate the oscillation directions. Thus the dependence of the torque acting on ψ is described by the function of $-\sin\psi$.

These phase-dependent torques lead to synchronization as follows. First, notice that the torque due to the stochastic input signal acting on the phase is inversely proportional to the oscillation amplitude s, as can be seen in the second term on the right-hand side in Eq. (11). This is because the phase change due to torque becomes large when the core is close to the pole (disk center); in fact, when the core is at the disk center, any small torque can change the phase from 0 to 2π. Therefore when the oscillation amplitude s is small, the torque due to the input signal becomes large and efficiently aligns the phases. Second, note that Eq. (11) depends on the oscillation amplitude s through the amplitude-phase coupling, described by the term ζs^2. The vortex cores oscillating with different amplitudes experience unequal torques, which reduce the separation between the core positions. The first explains the synchronization shown in Fig. 4(b), while the second one explains the synchronization in Fig. 4(c). Although these physical pictures are for a vortex STO, we believe that the considerations presented here are also applicable to the other STO types; see Appendix D.

These physical interpretations can be ascertained from a different viewpoint. Let us derive an analytical form for the Lyapunov exponent, which is an inverse of a timescale characterizing the evolution of the difference between two phases, $\delta\theta(t) = \theta_1(t) - \theta_2(t)$ as $|\delta\theta(t)| \simeq |\delta\theta(0)|e^{\lambda t}$. A negatively large Lyapunov exponent means that $\delta\theta(t)$ decays rapidly, i.e., a fast synchronization is achieved. We will use the phase reduction method developed in Refs. [36,42], which provides a general description of nonlinear oscillator systems and naturally includes the amplitude-phase coupling [14,15,27]. In particular, let us introduce a generalized phase θ, which changes with a time-independent frequency. As mentioned in Sec. II, the unperturbed Thiele equation has the same form as the Stuart-Landau oscillator. Therefore the generalized phase in the present system can be defined as

$$\theta = \psi + \frac{\zeta\kappa}{Gb}\ln\frac{s}{s_0}. \tag{12}$$

The concept of the phase reduction method developed in Ref. [36] is to describe any phenomena related to synchronization by the generalized phase, θ. The difference between ψ and θ is as follows. The phase ψ is the phase representing the vortex-core position in a polar coordinate. It changes with the frequency $f = (\kappa/G)(1+\zeta s^2)/(2\pi)$ as $\psi = 2\pi f t$. The frequency f of ψ clearly depends on the oscillation amplitude s. Therefore, while the frequency f in unperturbed limit-cycle state is $f_0 = (\kappa/G)(1+\zeta s_0^2)/(2\pi)$, as explained in Sec. II, an instantaneous frequency of the vortex core in the presence of a perturbation (random input signal in the present case) generally differs from f_0 because an instantaneous oscillation amplitude s could be different from s_0. On the other hand, the generalized phase used in the phase reduction method is defined so that it grows monotonically with a fixed frequency of f_0 even in the presence of perturbation [36], and thus an instantaneous s differs from s_0. To satisfy this requirement, we introduce θ defined by Eq. (12). It is also noticed that θ becomes identical to ψ on the limit-cycle trajectory, where $s = s_0$. The theory is applicable when the perturbation is small, while it is no longer applicable for large excitations such as noise-induced chaos [47]. The theory of phase reduction [36] argues that a response of a nonlinear oscillator to a weak perturbation can be described by the phase sensitivity function, which is defined as

$$\mathbf{Z}(\theta) = \nabla\theta|_{\mathbf{X}=\mathbf{X}_0}, \tag{13}$$

where $\mathbf{X}_0$ is the solution of the equation of motion in the unperturbed system, while ∇ is the gradient with respect to the spatial coordinate, $\mathbf{X}/R$, normalized by the disk radius R. In Eq. (12), $s = \sqrt{(X/R)^2 + (Y/R)^2}$ and $\psi = \tan^{-1}(Y/X)$ depend on $\mathbf{X}/R$. In the present case, the unperturbed solution is the vortex core rotating around the disk center with amplitude s_0 and frequency $(\kappa/G)(1+\zeta s_0^2)/(2\pi)$. Therefore the phase

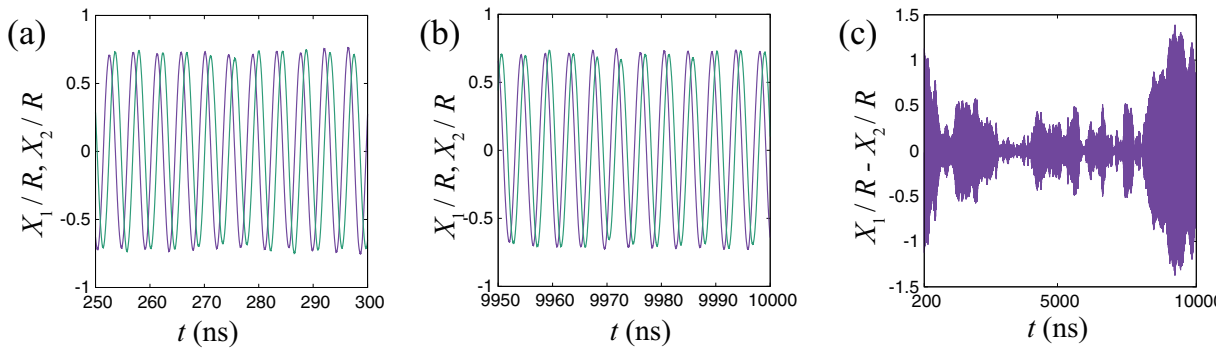

FIG. 7. (a), (b) Examples of oscillating behaviors of X/R in two trials (a) immediately after injection of the stochastic signal and (b) long after injection. The time evolution of their difference, $(X_1/R) - (X_2/R)$, is shown in (c). The maximum value of the input signal of the magnetic field is $h_x = 5.0$ Oe. The temperature is 300 K.

sensitivity function becomes

$$\mathbf{Z}(\theta) = \begin{pmatrix} \frac{1}{s_0}\left(-\sin\theta + \frac{\zeta\kappa}{Gb}\cos\theta\right) \\ \frac{1}{s_0}\left(\cos\theta + \frac{\zeta\kappa}{Gb}\sin\theta\right) \\ 0 \end{pmatrix}. \tag{14}$$

The equation of motion of the generalized phase in the presence of a stochastic input signal in the x direction becomes

$$\frac{d\theta}{dt} = \frac{\kappa}{G}(1+\zeta s_0^2) - \frac{c\mu^*}{GRs_0}h_x\mathcal{R}(t)\left(\sin\theta - \frac{\zeta\kappa}{Gb}\cos\theta\right). \tag{15}$$

Reference [42] developed a formula for the Lyapunov exponent λ of noise-induced synchronization in terms of the phase sensitivity function, where the input signal is assumed to be Gaussian noise. While pulse input signals are used in experiments on, for example, physical reservoir computing [50,51], it is convenient for us to assume Gaussian noise from a theoretical viewpoint. Note that the theory still provides a qualitative description of synchronization by a pulse input signal when the pulse width is sufficiently shorter than the oscillation period [58,59]; see also Appendix E. Therefore, for a while, let us replace the pulse input signal $h_x\mathcal{R}$ with a Gaussian one $\tilde{h}_x\tilde{\mathcal{R}}(t)$, where $\tilde{\mathcal{R}}(t)$ satisfies $\langle\tilde{\mathcal{R}}(t)\tilde{\mathcal{R}}(t')\rangle = \delta(t-t')$. Then, according to Ref. [42], the Lyapunov exponent becomes

$$\begin{aligned}\lambda &= -\frac{1}{4\pi}\left(\frac{c\mu^*\tilde{h}_x}{GR}\right)^2\int_0^{2\pi}d\theta\left(\frac{dZ_x}{d\theta}\right)^2 \\ &= -\left(\frac{c\mu^*\tilde{h}_x}{2GRs_0}\right)^2\left[1+\left(\frac{\zeta\kappa}{Gb}\right)^2\right].\end{aligned} \tag{16}$$

Equation (16) indicates that the Lyapunov exponent becomes negatively large when the oscillation amplitude s_0 is small or the amplitude-phase coupling ζ is large. It again explains the results of the numerical simulations shown in Fig. 4. In Appendix E we show the value of the Lyapunov exponent evaluated numerically and discuss a qualitative comparison with Eq. (16).

IV. SYNCHRONIZATION AT FINITE TEMPERATURE

Here we show the results of the numerical simulation on noise-induced synchronization at finite temperature. Recall that noise and stochastic input signal in previous sections mean (pseudo) random input, which can be applied to several oscillators simultaneously and/or reproducibly applied to an oscillator. On the other hand, the thermal fluctuation (or noise) added here originates from an internal nature of ferromagnet placed at finite temperature. The thermal fluctuation is independent among the oscillators and cannot be reproduced. In this sense, the stochastic input signal is sometimes called common input signal (or noise signal) [42], while the thermal fluctuation is independent noise.

A. Synchronized behavior

Let us first show the oscillatory behavior between two trials. Figures 7(a) and 7(b) respectively show the time evolutions of X/R in two trials immediately after injection of the stochastic input signal and a long time after injection. Figure 7(a) indicates that when only a short time has passed since injection of the stochastic input signal, the two trials are not synchronized, similar to what was found at zero temperature in Fig. 3(b). However, as can be seen in Fig. 7(b), even after a long time has passed, two trials still do not show synchronization. Figure 7(c) shows the time evolution of the difference between two X/R. Note that the difference is nonmonotonic, contrary to the monotonic decrease found at zero temperature in Fig. 3(d). Even after the difference becomes small, it randomly increases again. These results indicate that stochastic input signal causes synchronization, but thermal fluctuation causes desynchronization.

Next let us investigate the desynchronized behavior from another viewpoint. Figures 8(a)–8(c) show the time evolutions of the oscillation amplitude s of a single trial and its average for various values of I and ζ. In Fig. 8(a), the average amplitude sometimes becomes comparable to that of a single trial, indicating that synchronization is achieved. However, thermal fluctuation prevents the synchronized state from stabilizing, and thus the average amplitude often becomes smaller than that of a single trial. When the oscillation amplitude is small, the synchronized state remains for a relatively long time, as shown in Fig. 8(b). This is because the time necessary to achieve synchronization is relatively short, as explained in Fig. 5(b), and therefore, even when the vortex-core positions are randomly deviated, they immediately synchronize again. On the other hand, when the oscillation amplitude is large, the

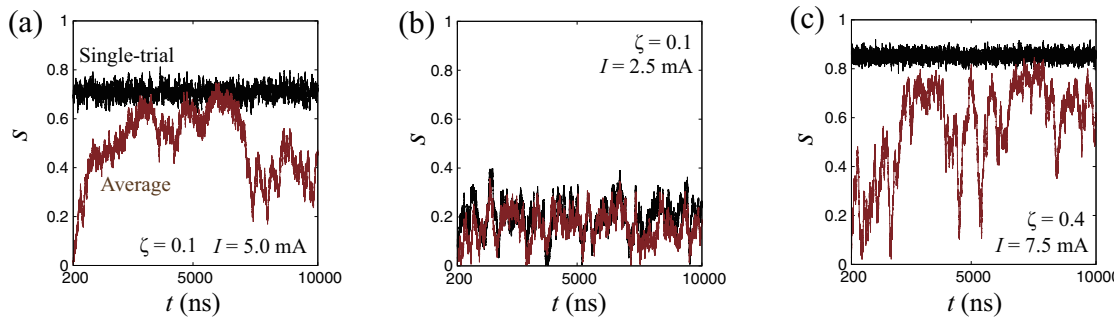

FIG. 8. Time evolutions of the oscillation amplitude s_0 of a single trial (black) and its average (brown), where the values of I and ζ are (a) 5.0 mA and 0.1, (b) 2.5 mA and 0.1, and (c) 7.5 mA and 0.4. The maximum value of the input signal of magnetic field is $h_x = 5.0$ Oe. The temperature is 300 K.

synchronized state is often broken even when the amplitude-phase coupling is large; see Fig. 8(c). This is because the time for synchronization is relatively long even at zero temperature, as explained in Fig. 5(c), and thermal fluctuation can easily prevent synchronization.

B. On-off intermittency

In the last section we showed that the thermal fluctuation prevents synchronization; see Figs. 8(a) and 8(c). Even when synchronization is realized, it is sometimes broken by the random torque, as shown in Fig. 8(b). This is in contrast to the synchronization at zero temperature in Fig. 5(b), where the synchronized state is sustained once it is realized. A transition between synchronized and desynchronized states, or equivalently, the appearance of a slip in the phase difference, has been found in a wide variety of nonlinear oscillators and is called on-off intermittency [35,42,60–68]. On-off intermittency is caused by a combination of a common input signal (stochastic magnetic field in the present system) or coupling and independent noise (thermal noise), and, for example, it triggers self-annealing that enhances the efficiency of learning in chaotic neural networks [69]. On-off intermittency is characterized by the statistical distribution of the interval between neighboring bursts, called the laminar length. Here we analyze the laminar length of noise-induced synchronization in STOs.

Figure 9(a) shows the time evolution of the phase difference $|\psi_1 - \psi_2|$ between two trials, where we use a relatively large value of h_x to realize synchronization frequently. Figure 9(b) shows the definition of the laminar length for the present case. Note that events with a short laminar length frequently happen. On the other hand, events with a long laminar length rarely happen. This does not necessarily mean that synchronization is absent; if synchronization is sustained, bursts rarely happen.

Figure 9(c) shows the distribution of laminar lengths in a relatively short-length region. To obtain this result, we use the 10 times of the simulation results between 3200 ns and 9600 ns. We find that the distribution obeys a power law with an exponent close to -1.5. The distribution in a relatively long length region, shown in Fig. 9(d), shows a deviation from the power law, which is partly due to the difficulty in observing events with a long laminar length, as mentioned above. Note that various oscillator systems have been found to have a similar power law [61,62,67], including the Stuart-Landau oscillator [42]. The similarity originates from the fact that the vortex-core dynamics described by the Thiele equation are mathematically similar in structure to the Stuart-Landau oscillator, as explained in Sec. II.

V. CONCLUSION

We investigated noise-induced synchronization in vortex STOs theoretically and found results that would be of interest to researchers in magnetism and nonlinear science. First, we performed a numerical simulation at zero temperature and

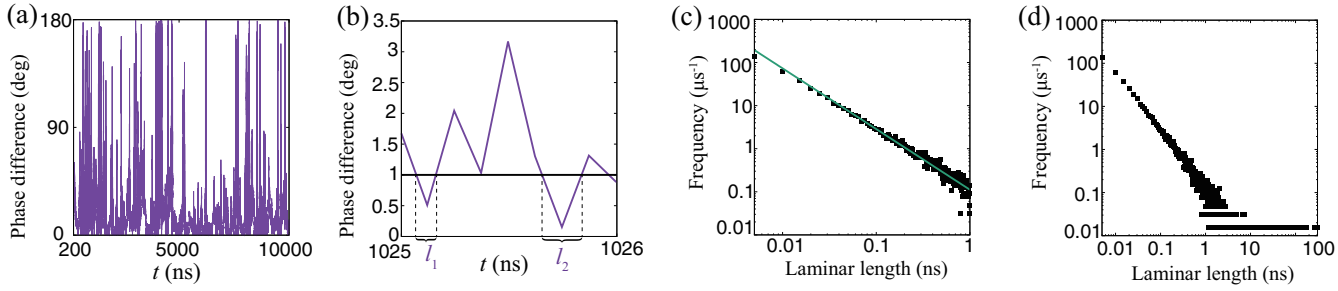

FIG. 9. (a) Absolute value of the phase difference, $|\psi_1 - \psi_2|$, between two trials, where $I = 2.5$ mA and $\zeta = 0.1$, and $h_x = 20$ Oe. The laminar length, l, is the interval between neighboring bursts. (b) Examples of the laminar length. The burst is a state in which the absolute value of the phase differences exceeds 1.0 degree. (c) Distribution of laminar lengths near the short-length region. The solid line represents the slope for an exponent of -1.5. (d) Distribution of laminar lengths over a wide range of lengths.

found that synchronization efficiently occurs when the oscillation amplitude is small and/or the amplitude-phase coupling is strong. Second, we developed an analytical theory of synchronization and revealed the physics behind the numerical results. The analytical form for the Lyapunov exponent implies that there are two ways to realize noise-induced synchronization. The first one is that the stochastic input signal provides a torque that directly affects the phase and leads to phase alignment, and the second is that the stochastic input signal changes the oscillation amplitude, which results in aligning the phases by changing the oscillation frequency. The first one leads to synchronization for small-amplitude oscillations while the second plays a role when the amplitude-phase coupling is finite. The oscillation amplitude can be controlled by the bias current magnitude, while the amplitude-phase coupling depends on the ferromagnetic materials. Therefore the results presented here provide directions for designing experiments in the future. Third, we performed a numerical simulation at finite temperature and found that thermal fluctuations cause on-off intermittency. A statistical analysis of the laminar length of the on-off intermittency reveals a power law similar to that of the different nonlinear oscillators found in nonlinear science.

ACKNOWLEDGMENTS

The results were partially obtained from the project "Innovative AI Chips and Next-Generation Computing Technology Development/(2) Development of Next-Generation Computing Technologies/Exploration of Neuromorphic Dynamics towards Future Symbiotic Society," commissioned by NEDO. K.N. is partially supported by JSPS KAKENHI Grant Number JP18H05472 and by JST CREST Grant Number JPMJCR2014, Japan. S.T. was partially supported by JST PREST (Grant Number JPMJPR20M5). T.T. is also supported by JPS KAKENHI through Grant Number 20H05655.

APPENDIX A: EXPLICIT FORMS OF THE THIELE EQUATION

The Thiele equation in terms of X and Y is explicitly given by

$$\dot{X} = a_s X - a_\psi Y + \frac{|D|(1+\xi s^2)}{G^2+(1+\xi s^2)^2 D^2}(ca_J J q_x R_0 - c\mu^* H_y) - \frac{G}{G^2+(1+\xi s^2)^2 D^2}(cb_J J q_x R - c\mu^* H_x) - \frac{|D|(1+\xi s^2)}{G^2+(1+\xi s^2)^2 D^2}\eta_x - \frac{G}{G^2+(1+\xi s^2)^2 D^2}\eta_y, \tag{A1}$$

$$\dot{Y} = a_\psi X + a_s Y - \frac{G}{G^2+(1+\xi s^2)^2 D^2}(ca_J J q_x R_0 - c\mu^* H_y) - \frac{|D|(1+\xi s^2)}{G^2+(1+\xi s^2)^2 D^2}(cb_J J q_x R - c\mu^* H_x) + \frac{G}{G^2+(1+\xi s^2)^2 D^2}\eta_x - \frac{|D|(1+\xi s^2)}{G^2+(1+\xi s^2)^2 D^2}\eta_y, \tag{A2}$$

where H_x and H_y are the x and y components of the magnetic field $\mathbf{H}$, and a_s and a_ψ are given by

$$a_s = \frac{G a_J J q_z - |D|\kappa(1+\xi s^2)(1+\zeta s^2)}{G^2+(1+\xi s^2)^2 D^2}, \tag{A3}$$

$$a_\psi = \frac{G\kappa(1+\zeta s^2) + |D|(1+\xi s^2) a_J J q_z}{G^2+(1+\xi s^2)^2 D^2}. \tag{A4}$$

In terms of s and ψ, the Thiele equation becomes

$$\dot{s} = a_s s + \frac{(ca_J J q_x R_0 - c\mu^* H_y)/R}{G^2+(1+\xi s^2)^2 D^2}[|D|(1+\xi s^2)\cos\psi - G\sin\psi] - \frac{(cb_J J q_x R - c\mu^* H_x)/R}{G^2+(1+\xi s^2)^2 D^2}[G\cos\psi + |D|(1+\xi s^2)\sin\psi] - \frac{G\eta_\psi/R}{G^2+(1+\xi s^2)^2 D^2} - \frac{|D|(1+\xi s^2)\eta_s/R}{G^2+(1+\xi s^2)^2 D^2}, \tag{A5}$$

$$\dot{\psi} = a_\psi - \frac{(ca_J J q_x R_0 - c\mu^* H_y)/R}{G^2+(1+\xi s^2)^2 D^2}[|D|(1+\xi s^2)\sin\psi + G\cos\psi]\frac{1}{s} + \frac{(cb_J J q_x R - c\mu^* H_x)/R}{G^2+(1+\xi s^2)^2 D^2}[G\sin\psi - |D|(1+\xi s^2)\cos\psi]\frac{1}{s} + \frac{G\eta_s/R}{G^2+(1+\xi s^2)^2 D^2}\frac{1}{s} - \frac{|D|(1+\xi s^2)\eta_\psi/R}{G^2+(1+\xi s^2)^2 D^2}\frac{1}{s}, \tag{A6}$$

where $\eta_s = \eta_x\cos\psi + \eta_y\sin\psi$ and $\eta_\psi = -\eta_x\sin\psi + \eta_y\cos\psi$ also satisfy the fluctuation-dissipation theorem, Eq. (3). Note that $|D|/G \simeq \alpha \ll 1$, and therefore the term $G^2+(1+\xi s^2)^2 D^2$ can be approximated as G^2. Note also

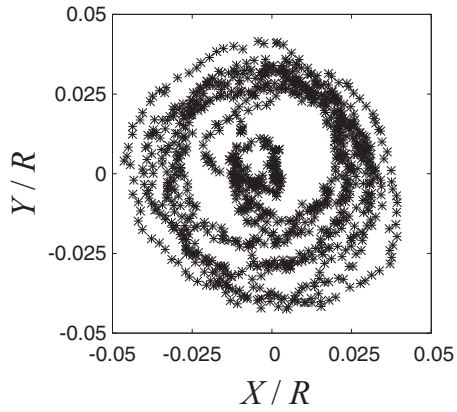

FIG. 10. Distribution of 1000 initial states near the disk center.

that $R_0/R \ll 1$; thus the terms related to $a_J J q_x R_0$ are small, which can be confirmed from the results in Fig. 2(a), where the oscillation amplitude of s in the steady state is small. Furthermore, the terms proportional to $\sin\psi$ and $\cos\psi$ become zero in an oscillating state after averaging over the oscillation period. Then, neglecting the magnetic field and random torque, Eqs. (A5) and (A6) reduce to Eqs. (4) and (5). Similarly, in the presence of a stochastic input signal through the magnetic field, the leading-order terms of Eqs. (A5) and (A6) provide Eqs. (10) and (11).

APPENDIX B: PREPARATION OF THE INITIAL STATES

We prepared 1000 initial states of the vortex core by numerically solving Eq. (1) in the absence of a current or field. The temperature was set to 300 K to obtain natural initial states of the vortex core. Figure 10 shows the distribution of initial states in the xy plane obtained in the numerical simulation, where the vortex cores stay near the disk center, which is an energetically stable state, and is randomly distributed due to thermal fluctuation. The temperature is set to 0 K after preparing the initial state when the numerical simulation is performed at zero temperature.

APPENDIX C: DEPENDENCE OF TIME FOR SYNCHRONIZATION ON STRENGTH OF INPUT SIGNAL

Here we show the dependence of the time for synchronization on the strength of input signal. Recall that Fig. 5(a) shows the time evolutions of the oscillation amplitude s and its average over 1000 trials at zero temperature for $I = 5.0$ mA, $\zeta = 0.1$, and $h_x = 5.0$ Oe. For comparison, these time evolutions are shown in Figs. 11(a) and 11(b) for $h_x = 2.5$ Oe and $h_x = 10$ Oe. The results indicate that fast synchronization is achieved when the strength of the input signal is large. We also performed similar numerical simulations at finite temperature. Here, when the strength of the input signal is small, the average oscillation amplitude does not saturate to that of a single trial, as shown in Fig. 11(c). Even when the strength of the input signal is large, the thermal fluctuation prevents a completely synchronized state and causes on-off intermittency, as shown in Fig. 11(d).

APPENDIX D: NOISE-INDUCED SYNCHRONIZATION IN MACROSPIN STO

The analytical theory developed in Sec. III indicates that there are two ways to realize noise-induced synchronization in STOs. The first one is that the input signal provides a torque directly leading phase alignment. The second one is that the input signal changes the oscillation amplitude, and the amplitude-phase (frequency) coupling leads to alignment of the phases. The first one works well when the vortex core is close to a pole, while the second becomes efficient when the amplitude-phase coupling is large. Although the results are for vortex STOs, we consider that the physical picture can be applied to the other types of STO qualitatively.

The insights provided above might solve a controversial issue in previous work. References [47,49] study noise-induced synchronization in macrospin STOs. While both papers focus on the same type of STO consisting of a perpendicularly magnetized free layer and an in-plane magnetized reference layer, Ref. [47] reported that noise-induced synchronization is achieved, while Ref. [49] argues that an additional magnetic anisotropy is necessary for realizing synchronization. Note that the stochastic input signal in these references is injected through the current and thus the spin-transfer torque provides stochastic torque.

First, note that Ref. [47] investigated the dynamics over a wide range of input intervals and strengths, while Ref. [49] studied a single set of parameters. Second, note that the first way in which the input signal directly aligns the phases seems to be inefficient because the oscillation occurs far away from the pole, which is the north pole along the perpendicular (z)

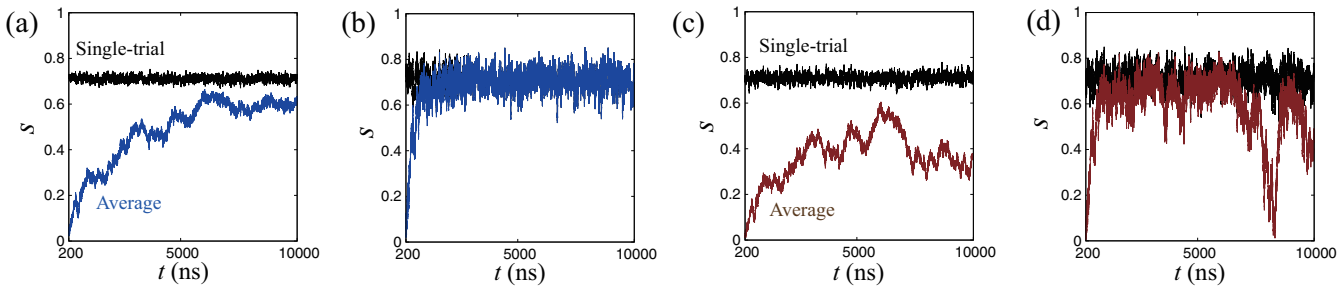

FIG. 11. Time evolutions of the oscillation amplitude s_0 of a single trial (black) and its average (blue) at zero temperature, where the maximum value of the input signal h_x is (a) 2.5 and (b) 10 Oe. Results at finite temperature are shown in (c) and (d). The values of I and ζ are 5.0 mA and 0.1, respectively.

direction in their geometry [47,49]. Note that the oscillation amplitude of the macrospin magnetization in Ref. [49] is relatively large; in fact, the magnetization oscillates almost entirely in the xy plane. Furthermore, the second way related to the amplitude-phase coupling becomes zero in the STO studied in Refs. [47,49], in contrast with the vortex STO where it remains finite. This difference arises from the magnetization alignment in Refs. [47,49]. Note that the oscillation amplitude of the STO in these references corresponds to the tilt angle of the macrospin magnetization from the z axis, which can be modulated by the current magnitude. As mentioned, the magnetization in the reference layer in Refs. [47,49] is in-plane magnetized. In such a case, when the macrospin magnetization comes close to the xy plane, the direction of the spin-transfer torque also lies in the xy plane. Therefore the stochastic input signal does not change the amplitude (tilted angle) efficiently. Accordingly, the second way does not work. Thus it was for this reason that noise-induced synchronization was not found in Ref. [49]. At the same time we should notice that the additional magnetic anisotropy prevents the magnetization from moving close to the xy plane, which makes the second way efficient. On the other hand, Ref. [47] found synchronization in the same type of STO because they investigated a wide range of current strengths. In a different geometry studied in Ref. [48], where the free layer is also in-plane magnetized, the spin-transfer torque can change the amplitude even in a large-amplitude oscillating state. Therefore noise-induced synchronization was also observed in that situation.

APPENDIX E: LYAPUNOV EXPONENT

Here we show the value of the Lyapunov exponent evaluated from the numerical simulation of the Landau-Lifshitz-Gilbert equation and compare it with Eq. (16). It will be shown that the formula explains the dependence of the Lyapunov exponent on the parameters qualitatively, although a quantitative comparison is difficult. This is because, as mentioned in Sec. III B, we use pulse input signals, as in the case of experiments, while it is convenient for theory to assume Gaussian noise.

Let us first explain the evaluation method of the Lyapunov exponent. We use a method similar to that developed in our past work [70], which is based on Ref. [71]. The inverse of the Lyapunov exponent is the timescale characterizing the evolution of the difference between two solutions of Eq. (1) with slightly different initial conditions. Therefore, at a certain time t_0, we introduce $\mathbf{u}^{(1)}(t_0) = \mathbf{x}(t_0) + \epsilon\mathbf{n}$, where $\mathbf{x}(t_0) = \mathbf{X}/R$ of Eq. (1). The factor $\epsilon\mathbf{n}$ represents $\mathbf{x}$ and $\mathbf{u}^{(1)}$, where $0 < \epsilon \ll 1$, and $\mathbf{n}$ is a unit vector pointing in an arbitrary direction. Both $\mathbf{x}(t_0)$ and $\mathbf{u}^{(1)}(t_0)$ evolve to $\mathbf{x}(t_0 + \Delta t)$ and $\mathbf{u}^{(1)}(t_0 + \Delta t)$, according to Eq. (1), where Δt is time increment of the numerical simulation. Since $\delta\mathbf{u}^{(1)} = \mathbf{u}^{(1)}(t_0 + \Delta t) - \mathbf{x}(t_0 + \Delta t)$ is the evolution of the difference between two solutions of Eq. (1), a temporal Lyapunov exponent at $t = t_0 + \Delta t$ is obtained as

$$\lambda^{(1)} = \frac{1}{\Delta t} \ln \frac{|\delta\mathbf{u}^{(1)}|}{\epsilon}. \tag{E1}$$

Next we define $\mathbf{u}^{(2)}(t_0 + \Delta t) = \mathbf{x}(t_0 + \Delta t) + (\epsilon/|\delta\mathbf{u}^{(1)}|)\,\delta\mathbf{u}^{(1)}$, which satisfies $|\mathbf{u}^{(2)}(t_0 + \Delta t) - \mathbf{x}(t_0 + \Delta t)| = \epsilon$. Solving Eq. (1), we obtain the temporal Lyapunov exponent at $t = t_0 + 2\Delta t$ as

$$\lambda^{(2)} = \frac{1}{\Delta t} \ln \frac{|\delta\mathbf{u}^{(2)}|}{\epsilon}, \tag{E2}$$

where $\delta\mathbf{u}^{(2)} = \mathbf{u}^{(2)}(t_0 + 2\Delta t) - \mathbf{x}(t_0 + 2\Delta t)$. In general, at $t = t_0 + n\Delta t$, we introduce $\mathbf{u}^{(n+1)}(t_0 + n\Delta t) = \mathbf{x}(t_0 + n\Delta t) + (\epsilon/|\delta\mathbf{u}^{(n)}|)\delta\mathbf{u}^{(n)}$ and evaluate the time evolutions of $\mathbf{x}(t_0 + n\Delta t)$ and $\mathbf{u}^{(n+1)}(t_0 + n\Delta t)$ to $\mathbf{x}[t_0 + (n+1)\Delta t]$ and $\mathbf{u}^{(n+1)}[t_0 + (n+1)\Delta t]$, respectively. Then the temporal Lyapunov exponent at $t = t_0 + (n+1)\Delta t$ is obtained as $\lambda^{(n+1)} = (1/\Delta t)\ln(|\delta\mathbf{u}^{(n+1)}|/\epsilon)$, where $\delta\mathbf{u}^{n+1} = \mathbf{u}^{(n+1)}[t_0 + (n+1)\Delta t] - \mathbf{x}[t_0 + (n+1)\Delta t]$. The Lyapunov exponent is obtained as

$$\lambda = \lim_{N\to\infty} \frac{1}{N} \sum_{i=1}^{N} \lambda^{(i)}. \tag{E3}$$

Note that Eq. (E3) corresponds to the first (or maximum) Lyapunov exponent, λ_1. In general, in an $\mathcal{M}$-dimensional phase space ($\mathcal{M} \in \mathbb{N}$), there are $\mathcal{M}$ Lyapunov exponents, $\lambda_1 \geqslant \lambda_2 \geqslant \cdots \geqslant \lambda_{\mathcal{M}}$. The value of Eq. (E3) is expected to be saturated to λ_1 and becomes independent from the choice of the direction $\mathbf{n}$ of the initial perturbation [71] because, repeating the procedure, the direction of the perturbation, $\delta\mathbf{u}^{(n)}$, naturally becomes parallel to the direction of the most expanded direction. Since the first Lyapunov exponent mainly determines the time necessary for synchronization in the present system, we call λ_1 the Lyapunov exponent and use the symbol λ, for simplicity. Note also that the present system is a nonautonomous system because of the presence of the time-dependent input signal. Equation (E3), strictly speaking, provides the conditional first Lyapunov exponent [47], which is restricted to the expansion rate of the vortex-core position, $\mathbf{X}$. In the present study we use $\epsilon = 1.0 \times 10^{-5}$ and $\Delta t = 5$ ps, $h_x = 15$ Oe, and $N = 4 \times 10^6$ pulses for the stochastic input signal. The perturbation is added starting from $t_0 = 200$ ns, i.e., the Lyapunov exponent is evaluated from the time at which the injection of stochastic input signal begins.

Figure 12(a) shows an example of the evolution of the Lyapunov exponent, i.e., $\lambda_1(t_0 + n\Delta t) = \sum_{i=1}^{n}(1/n)\lambda^{(i)}(t_0 + i\Delta t)$ when $I = 2.5$ mA and $\zeta = 0.1$. While it changes drastically at the initial stage due to an arbitrary choice of the direction of the initial perturbation, the value rapidly tends to saturate. Figure 12(b) shows the dependence of the Lyapunov exponent, numerically estimated by Eq. (E3), on the current I when $\zeta = 0.1$. The value of the Lyapunov exponent negatively increases with the current decreasing. Remember that s_0 in Eq. (16) depends on the current density J as $s_0 \propto \sqrt{J - J_c}$. Therefore the Lyapunov exponent in Eq. (16) is expected to become negatively large with the current magnitude decreasing, which is consistent with the numerically evaluated value in Fig. 12(b). The result shown in Fig. 12(b) appropriately reproduces this prediction. Figure 12(c) shows the dependence of the Lyapunov exponent on ζ when $I = 4.8$ mA, where the Lyapunov exponent, Eq. (E3), evaluated numerically increases with ζ increasing. Note that not only ζ explicitly appeared in Eq. (16) but also $s_0 \propto \sqrt{1/(\xi + \zeta)}$ and $b \propto (\xi + \zeta)$ affect the theoretical value in Eq. (16);

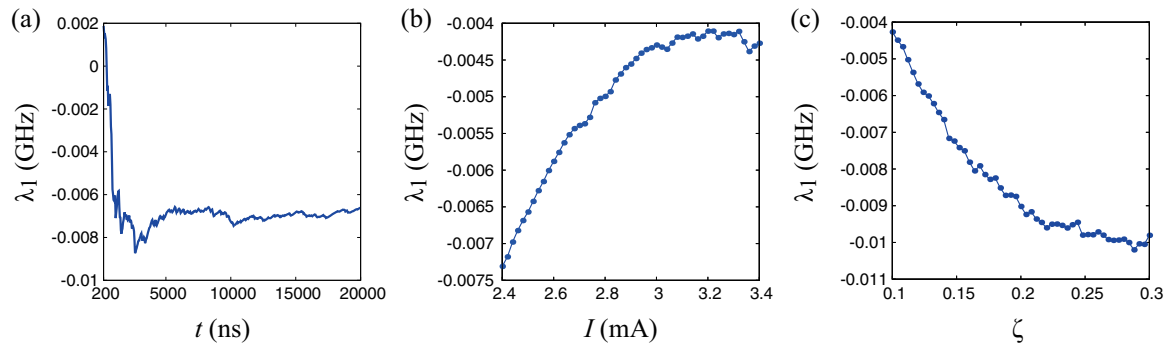

FIG. 12. (a) Time evolution of the Lyapunov exponent for $I = 2.5$ mA and $\zeta = 0.1$. Dependences of the Lyapunov exponent on (b) current I and (c) the amplitude-phase coupling parameter ζ, where $\zeta = 0.1$ in (b) and $I = 4.8$ mA in (c). The temperature is zero, while h_x is 15 Oe.

therefore the dependence is relatively complex. For the present parameter, however, the second term on the right-hand side is dominant, except $\zeta \simeq 0$, and the dependence of Eq. (16) on ζ is approximately given by $\zeta^2/(\xi + \zeta)$. Thus Eq. (16) predicts that the Lyapunov exponent negatively increases with ζ increasing, which is consistent with the numerical results in Fig. 12(c). Summarizing these results, we conclude that Eq. (16) well explains the dependence of the numerically evaluated Lyapunov exponent qualitatively and thus reflects the physics behind synchronization.

[1] J. C. Slonczewski, Current-driven excitation of magnetic multilayers, J. Magn. Magn. Mater. **159**, L1 (1996).

[2] L. Berger, Emission of spin waves by a magnetic multilayer traversed by a current, Phys. Rev. B **54**, 9353 (1996).

[3] J. C. Slonczewski, Currents, torques, and polarization factors in magnetic tunnel junctions, Phys. Rev. B **71**, 024411 (2005).

[4] S. I. Kiselev, J. C. Sankey, I. N. Krivorotov, N. C. Emley, R. J. Schoelkopf, R. A. Buhrman, and D. C. Ralph, Microwave oscillations of a nanomagnet driven by a spin-polarized current, Nature (London) **425**, 380 (2003).

[5] W. H. Rippard, M. R. Pufall, S. Kaka, T. J. Silva, and S. E. Russek, Current-driven microwave dynamics in magnetic point contacts as a function of applied field angle, Phys. Rev. B **70**, 100406(R) (2004).

[6] I. N. Krivorotov, N. C. Emley, J. C. Sankey, S. I. Kiselev, D. C. Ralph, and R. A. Buhrman, Time-domain measurements of nanomagnet dynamics driven by spin-transfer torques, Science **307**, 228 (2005).

[7] W. H. Rippard, M. R. Pufall, S. Kaka, T. J. Silva, S. E. Russek, and J. A. Katine, Injection Locking and Phase Control of Spin Transfer Nano-Oscillators, Phys. Rev. Lett. **95**, 067203 (2005).

[8] S. Kaka, M. R. Pufall, W. H. Rippard, T. J. Silva, S. E. Russek, and J. A. Katine, Mutual phase-locking of microwave spin torque nano-oscillators, Nature (London) **437**, 389 (2005).

[9] F. B. Mancoff, N. D. Rizzo, B. N. Engel, and S. Tehrani, Phase-locking in double-point-contact spin-transfer devices, Nature (London) **437**, 393 (2005).

[10] D. Houssameddine, U. Ebels, B. Delaët, B. Rodmacq, I. Firastrau, F. Ponthenier, M. Brunet, C. Thirion, J.-P. Michel, L. Prejbeanu-Buda, M.-C. Cyrille, O. Redon, and B. Dieny, Spin-torque oscillator using a perpendicular polarizer and a planer free layer, Nat. Mater. **6**, 447 (2007).

[11] J. Persson, Y. Zhou, and J. Akerman, Phase-locked spin torque oscillators: Impact of device variability and time delay, J. Appl. Phys. **101**, 09A503 (2007).

[12] U. Ebels, D. Houssameddine, I. Firastrau, D. Gusakova, C. Thirion, B. Dieny, and L. D. Buda-Prejbeanu, Macrospin description of the perpendicular polarizer-planar free-layer spin-torque oscillator, Phys. Rev. B **78**, 024436 (2008).

[13] A. M. Deac, A. Fukushima, H. Kubota, H. Maehara, Y. Suzuki, S. Yuasa, Y. Nagamine, K. Tsunekawa, D. D. Djayaprawira, and N. Watanabe, Bias-driven high-power microwave emission from MgO-based tunnel magnetoresistance devices, Nat. Phys. **4**, 803 (2008).

[14] G. Bertotti, I. Mayergoyz, and C. Serpico, *Nonlinear Magnetization Dynamics in Nanosystems* (Elsevier, Oxford, 2009).

[15] A. Slavin and V. Tiberkevich, Nonlinear auto-oscillator theory of microwave generation by spin-polarized current, IEEE. Trans. Magn. **45**, 1875 (2009).

[16] A. V. Khvalkovskiy, J. Grollier, A. Dussaux, K. A. Zvezdin, and V. Cros, Vortex oscillations induced by spin-polarized current in a magnetic nanopillar: Analytical versus micromagnetic calculations, Phys. Rev. B **80**, 140401(R) (2009).

[17] S. Urazhdin, P. Tabor, V. Tiberkevich, and A. Slavin, Fractional Synchronization of Spin-Torque Nano-Oscillators, Phys. Rev. Lett. **105**, 104101 (2010).

[18] T. J. Silva and M. W. Keller, Theory of thermally induced phase noise in spin torque oscillators for a high-symmetry case, IEEE Trans. Magn. **46**, 3555 (2010).

[19] W. H. Rippard, A. M. Deac, M. R. Pufall, J. M. Shaw, M. W. Keller, S. E. Russek, G. E. W. Bauer, and C. Serpico, Spin-transfer dynamics in spin valves with out-of-plane magnetized CoNi free layers, Phys. Rev. B **81**, 014426 (2010).

[20] A. Dussaux, B. Georges, J. Grollier, V. Cros, A. V. Khvalkovskiy, A. Fukushima, M. Konoto, H. Kubota, K. Yakushiji, S. Yuasa, K. A. Zvezdin, K. Ando, and A. Fert, Large microwave generation from current-driven magnetic vortex oscillators in magnetic tunnel junctions, Nat. Commun. **1**, 8 (2010).

[21] M. Quinsat, J. F. Sierra, I. Firastrau, V. Tiberkevich, A. Slavin, D. Gusakova, L. D. Buda-Prejbeanu, M. Zarudniev, J.-P. Michel, U. Ebels, B. Dieny, M.-C. Cyrille, J. A. Katine, D. Mauri, and A. Zeltser, Injection locking of tunnel junction oscillators to a microwave current, Appl. Phys. Lett. **98**, 182503 (2011).

[22] A. Dussaux, A. V. Khvalkovskiy, P. Bortolotti, J. Grollier, V. Cros, and A. Fert, Field dependence of spin-transfer-induced vortex dynamics in the nonlinear regime, Phys. Rev. B **86**, 014402 (2012).

[23] W. Rippard, M. Pufall, and A. Kos, Time required to injection-lock spin torque nanoscale oscillators, Appl. Phys. Lett. **103**, 182403 (2013).

[24] H. Kubota, K. Yakushiji, A. Fukushima, S. Tamaru, M. Konoto, T. Nozaki, S. Ishibashi, T. Saruya, S. Yuasa, T. Taniguchi, H. Arai, and H. Imamura, Spin-torque oscillator based on magnetic tunnel junction with a perpendicularly magnetized free layer and in-plane magnetized polarizer, Appl. Phys. Express **6**, 103003 (2013).

[25] T. Taniguchi, H. Arai, S. Tsunegi, S. Tamaru, H. Kubota, and H. Imamura, Critical field of spin torque oscillator with perpendicularly magnetized free layer, Appl. Phys. Express **6**, 123003 (2013).

[26] E. Grimaldi, A. Dussaux, P. Bortolotti, J. Grollier, G. Pillet, A. Fukushima, H. Kubota, K. Yakushiji, S. Yuasa, and V. Cros, Response to noise of a vortex based spin transfer nano-oscillator, Phys. Rev. B **89**, 104404 (2014).

[27] T. Taniguchi, Linewidth of power spectrum originated from thermal noise in spin torque oscillator, Appl. Phys. Express **7**, 053004 (2014).

[28] N. Locatelli, A. Hamadeh, F. A. Araujo, A. D. Belanovsky, P. N. Skirdkov, R. Lebrun, V. V. Naletov, K. A. Zvezdin, M. Munoz, J. Grollier, O. Klein, V. Cros, and G. de Loubens, Efficient synchronization of dipolarly coupled vortex-based spin transfer nano-oscillators, Sci. Rep. **5**, 17039 (2015).

[29] S. Tsunegi, K. Yakushiji, A. Fukushima, S. Yuasa, and H. Kubota, Microwave emission power exceeding 10 μW in spin torque vortex oscillator, Appl. Phys. Lett. **109**, 252402 (2016).

[30] S. Tsunegi, E. Grimaldi, R. Lebrun, H. Kubota, A. S. Jenkins, K. Yakushiji, A. Fukushima, P. Bortolotti, J. Grollier, S. Yuasa, and V. Cros, Self-injection locking of a vortex spin torque oscillator by delayed feedback, Sci. Rep. **6**, 26849 (2016).

[31] A. A. Awad, P. Dürrenfeld, A. Houshang, M. Dvornik, E. Iacoca, R. K. Dumas, and J. Akerman, Long-range mutual synchronization of spin Hall nano-oscillators, Nat. Phys. **13**, 292 (2017).

[32] S. Tsunegi, T. Taniguchi, R. Lebrun, K. Yakushiji, V. Cros, J. Grollier, A. Fukushima, S. Yuasa, and H. Kubota, Scaling up electrically synchronized spin torque oscillator networks, Sci. Rep. **8**, 13475 (2018).

[33] S. Tsunegi, T. Taniguchi, D. Suzuki, K. Yakushiji, A. Fukushima, S. Yuasa, and H. Kubota, Control of the stochastic response of magnetization dynamics in spin-torque oscillator through radio-frequency magnetic fields, Sci. Rep. **11**, 16285 (2021).

[34] S. H. Strogatz, *Nonlinear Dynamics and Chaos: With Applications to Physics, Biology, Chemistry, and Engineering*, 1st ed. (Westview Press, Boulder, CO, 2001).

[35] A. Pikovsky, M. Rosenblum, and J. Kurths, *Synchronization: A Universal Concept in Nonlinear Sciences*, 1st ed. (Cambridge University Press, Cambridge, England, 2003).

[36] Y. Kuramoto, *Chemical Oscillations, Waves, and Turbulence* (Dover, New York, 2003).

[37] K. Kudo, H. Suto, T. Nagasawa, K. Mizushima, and R. Sato, Resonant magnetization switching induced by spin-torque-driven oscillations and its use in three-dimensional magnetic storage applications, Appl. Phys. Express **8**, 103001 (2015).

[38] J. Torrejon, M. Riou, F. A. Araujo, S. Tsunegi, G. Khalsa, D. Querlioz, P. Bortolotti, V. Cros, K. Yakushiji, A. Fukushima, H. Kubota, S. Yuasa, M. D. Stiles, and J. Grollier, Neuromorphic computing with nanoscale spintronic oscillators, Nature (London) **547**, 428 (2017).

[39] Z. F. Mainen and T. J. Sejnowski, Reliability of spike timing in neocortical neurons, Science **268**, 1503 (1995).

[40] R. Toral, C. R. Mirasso, E. Hernández-García, and O. Piro, Analytical and numerical studies of noise-induced synchronization of chaotic systems, Chaos **11**, 665 (2001).

[41] D. S. Goldobin and A. Pikovsky, Synchronization and desynchronization of self-sustained oscillators by common noise, Phys. Rev. E **71**, 045201(R) (2005).

[42] J. N. Teramae and D. Tanaka, Robustness of the Noise-Induced Phase Synchronization in a General Class of Limit Cycle Oscillators, Phys. Rev. Lett. **93**, 204103 (2004).

[43] H. Nakao, K. Arai, and Y. Kawamura, Noise-Induced Synchronization and Clustering in Ensembles of Uncoupled Limit-Cycle Oscillators, Phys. Rev. Lett. **98**, 184101 (2007).

[44] W. F. Brown Jr., Thermal fluctuations of a single-domain particle, Phys. Rev. **130**, 1677 (1963).

[45] I. B. Yildiz, H. Jaeger, and S. J. Kiebel, Re-visiting the echo state property, Neural Networks **35**, 1 (2012).

[46] Z. Lu, B. R. Hunt, and E. Ott, Attractor reconstruction by machine learning, Chaos **28**, 061104 (2018).

[47] N. Akashi, T. Yamaguchi, S. Tsunegi, T. Taniguchi, M. Nishida, R. Sakurai, Y. Wakao, and K. Nakajima, Input-driven bifurcations and information processing capacity in spintronics reservoirs, Phys. Rev. Research **2**, 043303 (2020).

[48] K. Nakada, S. Yakata, and T. Kimura, Noise-induced transition of mutual synchronization in coupled spin torque nano oscillators, IEEE Trans. Magn. **48**, 4558 (2012).

[49] H. Arai and H. Imamura, Stochastic phase synchronization of perpendicularly magnetized spin-torque oscillators with the second-order uniaxial anisotropy, IEEE Trans. Magn. **53**, 6100705 (2017).

[50] S. Tsunegi, T. Taniguchi, S. Miwa, K. Nakajima, K. Yakusjiji, A. Fukushima, S. Yuasa, and H. Kubota, Evaluation of memory capacity of spin torque oscillator for recurrent neural networks, Jpn. J. Appl. Phys. **57**, 120307 (2018).

[51] S. Tsunegi, T. Taniguchi, K. Nakajima, S. Miwa, K. Yakushiji, A. Fukushima, S. Yuasa, and H. Kubota, Physical reservoir computing based on spin torque oscillator with forced synchronization, Appl. Phys. Lett. **114**, 164101 (2019).

[52] A. A. Thiele, Steady-State Motion of Magnetic Domains, Phys. Rev. Lett. **30**, 230 (1973).

[53] K. Y. Guslienko, X. F. Han, D. J. Keavney, R. Divan, and S. D. Bader, Magnetic Vortex Core Dynamics in Cylindrical Ferromagnetic Dots, Phys. Rev. Lett. **96**, 067205 (2006).

[54] K. Y. Guslienko, Low-frequency vortex dynamic susceptibility and relaxation in mesoscopic ferromagnetic dots, Appl. Phys. Lett. **89**, 022510 (2006).

[55] B. A. Ivanov and C. E. Zaspel, Excitation of Spin Dynamics by Spin-Polarized Current in Vortex State Magnetic Disks, Phys. Rev. Lett. **99**, 247208 (2007).

[56] K. Y. Guslienko, G. R. Aranda, and J. Gonzalez, Spin torque and critical currents for magnetic vortex nano-oscillator in nanopillars, J. Phys.: Conf. Ser. **292**, 012006 (2011).

[57] N. Rulkov, M. M. Sushchik, L. S. Tsimring, and H. D. I. Abarbanel, Generalized synchronization of chaos in directionally coupled chaotic systems, Phys. Rev. E **51**, 980 (1995).

[58] J.-N. Teramae and D. Tanaka, Noise induced phase synchronization of a general class of limit cycle oscillators, Prog. Theor. Phys. Suppl. **161**, 360 (2006).

[59] W. Kurebayashi, K. Fujiwara, and T. Ikeguchi, Colored noise induces synchronization of limit cycle oscillators, Europhys. Lett. **97**, 50009 (2012).

[60] N. Platt, E. A. Spiegel, and C. Tresser, On-Off Intermittency: A Mechanism for Bursting, Phys. Rev. Lett. **70**, 279 (1993).

[61] J. F. Heagy, N. Platt, and S. M. Hammel, Characterization of on-off intermittency, Phys. Rev. E **49**, 1140 (1994).

[62] P. W. Hammer, N. Platt, S. M. Hammel, J. F. Heagy, and B. D. Lee, Experimental Observation of On-Off Intermittency, Phys. Rev. Lett. **73**, 1095 (1994).

[63] Y. H. Yu, K. Kwak, and T. K. Lim, On-off intermittency in an experimental synchronization process, Phys. Lett. A **198**, 34 (1995).

[64] F. Rödelsperger, A. Čenys, and H. Benner, On-Off Intermittency in Spin-Wave Instabilities, Phys. Rev. Lett. **75**, 2594 (1995).

[65] A. Čenys, A. Namajūnas, A. Tamaševičius, and T. Schneider, On-off intermittency in chaotic synchronization experiment, Phys. Lett. A **213**, 259 (1996).

[66] J. W. Shuai and K. W. Wong, Noise and synchronization in chaotic neural networks, Phys. Rev. E **57**, 7002 (1998).

[67] S. Rim, D.-U. Hwang, I. Kim, and C.-M. Kim, Chaotic Transition of Random Dynamical Systems and Chaos Synchronization by Common Noise, Phys. Rev. Lett. **85**, 2304 (2000).

[68] A. N. Pisarchik and V. J. Pinto-Robledo, Experimental observation of two-state on-off intermittency, Phys. Rev. E **66**, 027203 (2002).

[69] M. Inoue and A. Nagayoshi, Solving an optimization problem with a chaos neural network, Prog. Theor. Phys. **88**, 769 (1992).

[70] T. Taniguchi, N. Akashi, H. Notsu, M. Kimura, H. Tsukahara, and K. Nakajima, Chaos in nanomagnet via feedback current, Phys. Rev. B **100**, 174425 (2019).

[71] I. Shimada and T. Nagashima, A numerical approach to ergodic problem of dissipative dynamical systems, Prog. Theor. Phys. **61**, 1605 (1979).